Metal Ion-Catalyzed Cycloaddition vs Hydride Transfer Reactions of NADH Analogues with *p*-Benzoquinones

Shunichi Fukuzumi,* Yoshinori Fujii, and Tomoyoshi Suenobu

Contribution from the Department of Material and Life Science, Graduate School of Engineering, Osaka University, CREST, Japan Science and Technology Corporation (JST), Suita, Osaka 565-0871, Japan

Received June 8, 2001

Abstract: 1-Benzyl-4-*tert*-butyl-1,4-dihydronicotinamide (*t*-BuBNAH) reacts efficiently with *p*-benzoquinone (Q) to yield a [2+3] cycloadduct (**1**) in the presence of $Sc(OTf)_3$ (OTf = OSO_2CF_3) in deaerated acetonitrile (MeCN) at room temperature, while no reaction occurs in the absence of Sc^{3+}. The crystal structure of **1** has been determined by the X-ray crystal analysis. When *t*-BuBNAH is replaced by 1-benzyl-1,4-dihydronicotinamide (BNAH), the Sc^{3+}-catalyzed cycloaddition reaction of BNAH with Q also occurs to yield the [2+3] cycloadduct. Sc^{3+} forms 1:4 complexes with *t*-BuBNAH and BNAH in MeCN, whereas there is no interaction between Sc^{3+} and Q. The observed second-order rate constant (k_{obs}) shows a first-order dependence on [Sc^{3+}] at low concentrations and a second-order dependence at higher concentrations. The first-order and the second-order dependence of the rate constant (k_{et}) on [Sc^{3+}] was also observed for the Sc^{3+}-promoted electron transfer from CoTPP (TPP = tetraphenylporphyrin dianion) to Q. Such dependence of k_{et} on [Sc^{3+}] is ascribed to formation of 1:1 and 1:2 complexes between $Q^{\bullet-}$ and Sc^{3+} at the low and high concentrations of Sc^{3+}, respectively, which results in acceleration of the rate of electron transfer. The formation constants for the 1:2 complex (K_2) between the radical anions of a series of *p*-benzoquinone derivatives ($X-Q^{\bullet-}$) and Sc^{3+} are determined from the dependence of k_{et} on [Sc^{3+}]. The K_2 values agree well with those determined from the dependence of k_{obs} on [Sc^{3+}] for the Sc^{3+}-catalyzed addition reaction of *t*-BuBNAH and BNAH with X−Q. Such an agreement together with the absence of the deuterium kinetic isotope effects indicates that the addition proceeds via the Sc^{3+}-promoted electron transfer from *t*-BuBNAH and BNAH to Q. When $Sc(OTf)_3$ is replaced by weaker Lewis acids such as $Lu(OTf)_3$, $Y(OTf)_3$, and $Mg(ClO_4)_2$, the hydride transfer reaction from BNAH to Q also occurs besides the cycloaddition reaction and the k_{obs} value decreases with decreasing the Lewis acidity of the metal ion. Such a change in the type of reaction from a cycloaddition to a hydride transfer depending on the Lewis acidity of metal ions employed as a catalyst is well accommodated by the common reaction mechanism featuring the metal-ion promoted electron transfer from BNAH to Q.

Introduction

Mechanisms of hydride transfer reactions of nicotinamide adenine dinucleotide (NADH) analogues with hydride acceptors such as carbonyl compounds and organic cations have been extensively studied chemically[1−8] or electrochemically.[9,10] The effects of metal ions on hydride transfer reactions from NADH analogues to substrates have particularly attracted considerable interest in relation to the essential role of metal ions in the redox reactions of nicotinamide coenzymes in the native enzymatic system.[1−4,11,12] Metal ions acting as Lewis acids have been reported to accelerate electron-transfer reactions, where metal ions bind to the product radical anions produced in the electron-

* Author to whom correspondence should be addressed.

(1) (a) Eisner, U.; Kuthan, J. *Chem. Rev.* **1972**, *72*, 1. (b) Stout, D. M.; Meyers, A. I. *Chem. Rev.* **1982**, *82*, 223.

(2) (a) Sund, H. *Pyridine-Nucleotide Dependent Dehydrogenase*; Walter de Gruyer: West Berlin, Germany, 1977. (b) Kellog, R. M. *Top. Curr. Chem.* **1982**, *101*, 111. Kellog, R. M. *Angew. Chem.* **1984**, *96*, 769. (c) Ohno, A.; Ushida, S. In *Lecture Notes in Bioorganic Chemistry, Mechanistic Models of Asymmetric Reductions;* Springer-Verlag: Berlin, Germany, 1986; p 105. (d) Bunting, J. W. *Bioorg. Chem.* **1991**, *19*, 456. (e) He, G.-X.; Blasko, A.; Bruice, T. C. *Bioorg. Chem.* **1993**, *21*, 423. (f) Ohno, A. *J. Phys. Org. Chem.* **1995**, *8*, 567.

(3) (a) Fukuzumi, S. In *Advances in Electron-Transfer Chemistry*; Mariano, P. S., Ed.; JAI Press; Greenwich, CT, 1992; pp 67−175. (b) Fukuzumi, S.; Tanaka, T. In *Photoinduced Electron Transfer*; Fox, M. A., Chanon, M., Eds.; Elsevier: Amsterdam, The Netherlands, 1988; Part C, Chapter 10.

(4) (a) Fukuzumi, S.; Koumitsu, S.; Hironaka, K.; Tanaka, T. *J. Am. Chem. Soc.* **1987**, *109*, 305. (b) Fukuzumi, S.; Mochizuki, S.; Tanaka, T. *J. Am. Chem. Soc.* **1989**, *111*, 1497. (c) Fukuzumi, S.; Kitano, T.; Ishikawa, M. *J. Am. Chem. Soc.* **1990**, *112*, 5631. (d) Fukuzumi, S.; Tokuda, Y.; Kitano, T.; Okamoto, T.; Otera, J. *J. Am. Chem. Soc.* **1993**, *115*, 8960. (e) Fukuzumi, S.; Ohkubo, K.; Tokuda, Y.; Suenobu, T. *J. Am. Chem. Soc.* **2000**, *122*, 4286.

(5) (a) Cheng, J.-P.; Lu, Y.; Zhu, X.; Mu, L. *J. Org. Chem.* **1998**, *63*, 6108. (b) Pestovsky, O.; Bakac, A.; Espenson, J. H. *J. Am. Chem. Soc.* **1998**, *120*, 13422. (c) Coleman, C. A.; Rose, J. G.; Murray, C. J. *J. Am. Chem. Soc.* **1992**, *114*, 9755. (d) Murray, C. J.; Webb, T. *J. Am. Chem. Soc.* **1991**, *113*, 7426. (e) Cheng, J.-P.; Handoo, K. L.; Xue, J.; Parker, V. D. *J. Org. Chem.* **1993**, *58*, 5050.

(6) (a) Carlson, B. W.; Miller, L. L.; Neta, P.; Grodkowski, J. *J. Am. Chem. Soc.* **1984**, *106*, 7233. (b) Powell, M. F.; Wu, J. C.; Bruice, T. C. *J. Am. Chem. Soc.* **1984**, *106*, 3850. (c) Sinha, A.; Bruice, T. C. *J. Am. Chem. Soc.* **1984**, *106*, 7291.

(7) (a) Tanner, D. D.; Kharrat, A.; Oumar-Mahamat, H. *Can. J. Chem.* **1990**, *68*, 1662. (b) Tanner, D. D.; Kharrat, A. *J. Org. Chem.* **1988**, *53*, 1646. (c) Liu, Y.-C.; Li, B.; Guo, Q.-X. *Tetrahedron* **1995**, *51*, 9671. (d) Ohno, A.; Ishikawa, Y.; Yamazaki, N.; Okamura, M.; Kawai, Y. *J. Am. Chem. Soc.* **1998**, *120*, 1186. (e) Kanomata, N.; Nakata, T. *Angew. Chem., Int. Ed. Engl.* **1997**, *36*, 1207. (f) Kanomata, N.; Suzuki, M.; Yoshida, M.; Nakata, T. *Angew. Chem., Int. Ed. Engl.* **1998**, *37*, 1410. (g) Konno, H.; Sakamoto, K.; Ishitani, O. *Angew. Chem., Int. Ed.* **2000**, *39*, 4061.

(8) (a) Kreevoy, M. M.; Ostović, D.; Lee, I.-S. H.; Binder, D. A.; King, G. W. *J. Am. Chem. Soc.* **1988**, *110*, 524. (b) Lee, I.-S. H.; Jeoung, E. H.; Kreevoy, M. M. *J. Am. Chem. Soc.* **1997**, *119*, 2722.

10.1021/ja016370k CCC: $20.00
Published on Web 09/27/2001

transfer reactions.[13−16] Both thermal and photochemical redox reactions which would otherwise be unlikely to occur have been made possible efficiently by the catalysis of metal ions on the rate-determining electron-transfer steps.[13−16] Among metal ions, rare-earth metal ions have attracted much attention as much more effective Lewis acids than divalent metal ions such as Mg^{2+} and Zn^{2+} in various carbon−carbon bond forming reactions due to the strong affinity to carbonyl oxygen.[17−19] However, there has been no report on rare-earth metal ion-catalyzed reactions of NADH analogues.

We report herein that novel and efficient [2+3] cycloaddition reactions of NADH analogues with *p*-benzoquinone derivatives rather than the hydride transfer reactions occur in the presence of scandium triflate ($Sc(OTf)_3$) in MeCN. When 1-benzyl-4-*tert*-butyl-1,4-dihydronicotinamide (*t*-BuBNAH) is used as an NADH analogue in the Sc^{3+}-catalyzed reaction with *p*-benzoquinone, the crystal structure of the cycloadduct was determined successfully. The cycloaddition of 1,4-dihydropyridine derivatives with *p*-benzoquinones has been reported in dioxane solution in the presence of $HClO_4$,[20] where BNAH is unstable toward acid-catalyzed hydrolysis.[21] There exist a few other reports concerning the addition reaction of BNAH or substituted BNAH with carbonyl compounds.[22] However, neither definitive characterization of the adducts nor the catalytic mechanism has so far been reported. The kinetic analysis of the Sc^{3+}-catalyzed cycloaddition reactions involving kinetic deuterium isotope effects as compared to the authentic electron-transfer reactions provides valuable information for the catalytic mechanisms of Sc^{3+}. The effects of other metal ions have also been studied in comparison with the catalytic effect of Sc^{3+} to reveal the relation between the cycloaddition and the hydride transfer reactions of NADH analogues.

Experimental Section

Materials. Preparation of 1-benzyl-1,4-dihydronicotinamide (BNAH) was described previously.[23] The dideuterated compound, 1-benzyl-1,4-dihydro[4,4′-$^2H_2$]nicotinamide (BNAH-4,4′-d_2), was prepared from monodeuterated compound (BNAH-4-d_1)[24] by three cycles of oxidation with *p*-chloranil in dimethylformamide and reduction with dithionite in deuterium oxide.[25] The deuterated *p*-benzoquinone (*p*-benzoquinone-d_4) was obtained commercially from Aldrich and used as received. The *tert*-butylated BNAH (*t*-BuBNAH) was prepared by the Grignard reaction with BNA^+Cl^- and purified by recrystallization from ethanol.[26,27] The BNA dimer was prepared according to the literature.[28,29] Cobalt(II) tetraphenylporphyrin (CoTPP) was prepared as given in the literature.[30] Scandium triflate [$Sc(OTf)_3$] was prepared by the following procedure according to the literature.[31] A deionized aqueous solution was mixed (1:1 v/v) with trifluoromethanesulfonic acid (>99.5%, 10.6 mL) obtained from Central Glass, Co., Ltd., Japan. The trifluoromethanesulfonic acid solution was slowly added to a flask which contained scandium oxide (Sc_2O_3) (> 99.9%, 30 mmol) obtained from Shin Etsu Chemical, Co., Ltd., Japan. The mixture was refluxed at 100 °C for 3 days. After centrifugation, the solution containing scandium triflate was separated and water was removed by vacuum evaporation. Scandium triflate was dried under vacuum evacuation at 403 K for 40 h. Similarly, lutetium triflate and yttrium triflate were prepared by the reaction of lutetium oxide and yttrium oxide with an aqueous trifluormethanesulfonic acid solution. Anhydrous magnesium perchlo-

(9) (a) Anne, A.; Fraoua, S.; Grass, V.; Moiroux, J.; Savéant, J.-M. *J. Am. Chem. Soc.* **1998**, *120*, 2951. (b) Anne, A.; Fraoua, S.; Moiroux, J.; Savéant, J.-M. *J. Am. Chem. Soc.* **1996**, *118*, 3938. (c) Anne, A.; Fraoua, S.; Hapiot, P.; Moiroux, J.; Savéant, J.-M. *J. Am. Chem. Soc.* **1995**, *117*, 7412. (d) Hapiot, P.; Moiroux, J.; Savéant, J.-M. *J. Am. Chem. Soc.* **1990**, *112*, 1337. (e) Anne, A.; Hapiot, P.; Moiroux, J.; Neta, P.; Savéant, J.-M. *J. Phys. Chem.* **1991**, *95*, 2370. (f) Anne, A.; Hapiot, P.; Moiroux, J.; Neta, P.; Savéant, J.-M. *J. Am. Chem. Soc.* **1992**, *114*, 4694. (g) Anne, A.; Moiroux, J.; Savéant, J.-M. *J. Am. Chem. Soc.* **1993**, *115*, 10224.

(10) (a) Miller, L. L.; Valentine, J. R. *J. Am. Chem. Soc.* **1988**, *110*, 3982. (b) Klippenstein, J.; Arya, P.; Wayner, D. D. M. *J. Org. Chem.* **1991**, *56*, 6736. (c) Bunting, J. W.; Stefanidis, D. *J. Org. Chem.* **1986**, *51*, 2060. (d) Carlson, B. W.; Miller, L. L. *J. Am. Chem. Soc.* **1985**, *107*, 479. (e) Bardea, A.; Katz, E.; Bückmann, A. F.; Willner, I. *J. Am. Chem. Soc.* **1997**, *119*, 9114.

(11) (a) Sigman, D. S.; Hajdu, J.; Creighton, D. J. In *Bioorganic Chemistry*; van Tamelen, E. E., Ed.; Academic Press: New York, 1978; Vol. IV, p 385. (b) Gase, R. A.; Pandit, U. K. *J. Am. Chem. Soc.* **1979**, *101*, 7059. (c) Ohno, A.; Yamamoto, H.; Oka, S. *J. Am. Chem. Soc.* **1981**, *103*, 2041. (d) Ohno, A.; Shio, T.; Yamamoto, H.; Oka, S. *J. Am. Chem. Soc.* **1981**, *103*, 2045.

(12) (a) Fukuzumi, S.; Nishizawa, N.; Tanaka, T. *J. Chem. Soc., Perkin Trans. 2* **1985**, 371. (b) Ishikawa, M.; Fukuzumi, S. *J. Chem. Soc., Faraday Trans.* **1990**, *86*, 3531.

(13) (a) Fukuzumi, S. *Bull. Chem. Soc. Jpn.* **1997**, *70*, 1. (b) Fukuzumi, S.; Itoh, S. In *Advances in Photochemistry*; Neckers, D. C., Volman, D. H., von Bünau, G., Eds.; Wiley: New York, 1998; Vol. 25, pp 107−172.

(14) Fukuzumi, S. In *Electron Transfer in Chemistry*; Balzani, V., Ed.; Wiley-VCH: Weinheim, Germany, 2001; Vol. 4, pp 3−59.

(15) (a) Fukuzumi, S.; Okamoto, T. *J. Am. Chem. Soc.* **1993**, *115*, 11600. (b) Itoh, S.; Kawakami, H.; Fukuzumi, S. *J. Am. Chem. Soc.* **1998**, *120*, 7271. (c) Itoh, S.; Kawakami, H.; Fukuzumi, S. *J. Am. Chem. Soc.* **1997**, *119*, 439. (d) Itoh, S.; Kawakami, H.; Fukuzumi, S. *Biochemistry* **1998**, *37*, 6562.

(16) (a) Fukuzumi, S.; Okamoto, T.; Otera, J. *J. Am. Chem. Soc.* **1994**, *116*, 5503. (b) Fukuzumi, S.; Tanaka, T. In *Photoinduced Electron Transfer*; Fox, M. A., Chanon, M., Eds.; Elsevier: Amsterdam, The Netherlands, 1988; Part C, Chapter 11, pp 636−687.

(17) (a) Kagan, H. B.; Namy, J. L. *Tetrahedron* **1986**, *42*, 6573. (b) Molander, G. A. *Chem. Rev.* **1992**, *92*, 29. (c) Imamoto, T. *Lanthanides in Organic Synthesis*; Katritzky, A. R., Meth-Cohn, O., Rees, C. W., Eds.; Academic Press: London, UK, 1994. (d) Kobayashi, S. *Synlett* **1994**, 689. (e) Marshmann, R. W. *Aldrichim. Acta* **1995**, *28*, 77. (f) Inanaga, J.; Yamaguchi, M. In *New Aspects of Organic Chemistry*; Yoshida, Z., Shiba, T., Ohshiro, Y., Eds.; VCH: New York, 1989; Chapter 4, p 55. (g) Molander, G. A.; Harris, C. R. *Chem. Rev.* **1996**, *96*, 307. (h) Shibasaki, M.; Sasai, H.; Arai, T. *Angew. Chem., Int. Ed. Engl.* **1997**, *36*, 1236.

(18) (a) Kobayashi, S.; Nagayama, S.; Busujima, T. *J. Am. Chem. Soc.* **1998**, *120*, 8287. (b) Kobayashi, S.; Ishitani, H. *J. Am. Chem. Soc.* **1994**, *116*, 4083. (c) Markó, I. E.; Evans, G. R. *Tetrahedron Lett.* **1994**, *35*, 2771. (d) Kawada, A.; Mitamura, S.; Kobayashi, S. *Chem. Commun.* **1996**, 183. (e) Kobayashi, S.; Araki, M.; Hachiya, I. *J. Org. Chem.* **1994**, *59*, 3758.

(19) (a) Ishihara, K.; Kubota, M.; Kurihara, H.; Yamamoto, H. *J. Org. Chem.* **1996**, *61*, 4560. (b) Ishihara, K.; Kubota, M.; Kurihara, H.; Yamamoto, H. *J. Am. Chem. Soc.* **1995**, *117*, 4413, 6639. (c) Kobayashi, S.; Nagayama, S. *J. Am. Chem. Soc.* **1998**, *120*, 2985. (d) Kobayashi, S.; Hachiya, I.; Araki, M.; Ishitani, H. *Tetrahedron Lett.* **1993**, *34*, 3755. (e) Kawada, A.; Mitamura, S.; Kobayashi, S. *Synlett* **1994**, 689. (f) Kobayashi, S.; Moriwaki, M.; Hachiya, I. *J. Chem. Soc., Chem. Commun.* **1995**, 1527. (g) Kobayashi, S.; Nagayama, S. *J. Org. Chem.* **1996**, *61*, 2256. (h) Kobayashi, S.; Nagayama, S. *J. Am. Chem. Soc.* **1996**, *118*, 8977. (i) Bisi Castellani, C.; Carugo, O.; Giusti, M.; Leopizzi, C.; Perotti, A.; Invernizzi Gamba, A.; Vidari, G. *Tetrahedron* **1996**, *52*, 11045. (j) Lacôte, E.; Renaud, P. *Angew. Chem., Int. Ed. Engl.* **1998**, *37*, 2259.

(20) (a) Hilgeroth, A.; Kuna, K.; Kuckländer, U. *Heterocycles* **1998**, *48*, 1649. (b) Hilgeroth, A.; Brachwitz, K.; Baumeister, U. *Heterocycles* **2001**, *55*, 661.

(21) (a) van Eikeren, P.; Grier, D. L.; Eliason, J. *J. Am. Chem. Soc.* **1979**, *101*, 7406. (b) Kim, C. S. Y.; Chaykin, S. *Biochemistry* **1968**, *7*, 2339. (c) Fukuzumi, S.; Ishikawa, M.; Tanaka, T. *Tetrahedron* **1986**, *42*, 1021.

(22) (a) Tagaki, W.; Sakai, H.; Yano, Y.; Ozeki, K.; Shimizu, Y. *Tetrahedron Lett.* **1976**, 2541. (b) Powell, M. F.; Bruice, T. C. *J. Am. Chem. Soc.* **1983**, *105*, 7139.

(23) Fukuzumi S.; Koumitsu, S.; Hironaka, K.; Tanaka, T. *J. Am. Chem. Soc.* **1987**, *109*, 305.

(24) (a) Anderson, A. G., Jr.; Berkelhammer, G. *J. Am. Chem. Soc.* **1958**, *80*, 992. (b) Mauzerall, D.; Westheimer, F. H. *J. Am. Chem. Soc.* **1955**, *77*, 2261.

(25) Caughey, W. S.; Schellenberg, K. A. *J. Org. Chem.* **1966**, *31*, 1978.

(26) Anne, A. *Heterocycles* **1992**, *34*, 2331.

(27) Takada, N.; Itoh, S.; Fukuzumi, S. *Chem. Lett.* **1996**, 1103.

(28) Wallenfels, K.; Gellerich, M. *Chem. Ber.* **1959**, *92*, 1406.

(29) Patz, M.; Kuwahara, Y.; Suenobu, T.; Fukuzumi, S. *Chem. Lett.* **1997**, 567.

(30) Shirazi, A.; Goff, H. M. *Inorg. Chem.* **1982**, *21*, 3420.

(31) (a) Forsberg, J. H.; Spaziano, V. T.; Balasubramanian, T. M.; Liu, G. K.; Kinsley, S. A.; Duckworth, C. A.; Poteruca, J. J.; Brown, P. S.; Miller, J. L. *J. Org. Chem.* **1987**, *52*, 1017. (b) Kobayashi, S.; Hachiya, I. *J. Org. Chem.* **1994**, *59*, 3590. (c) Kobayashi, S.; Hachiya, I.; Ishitani, H.; Araki, M. *Synlett* **1993**, 472. (d) Thom, K. F. U.S. Patent 3615169, 1971; *Chem. Abstr.* **1972**, *76*, 5436a.

Table 1. Summary of X-ray Crystallographic Data of the Cycloadduct (**1**)

compound	*t*-BuBNAH-Q
empirical formula	$C_{25}H_{31}N_2O_{3.5}$
formula weight	415.53
crystal system	monoclinic
space group	*C*2/*c* (no. 15)
a, Å	28.519(8)
b, Å	14.996(3)
c, Å	10.628(3)
α, deg	
β, deg	96.35(3)
γ, deg	
V, Å^3	4517(2)
Z	8
F(000)	1784.00
D_{calc}, g/cm^3	1.222
T, °C	23.0
crystal size, mm	0.20 × 0.20 × 0.40
μ(Mo Kα), cm^{-1}	0.81
diffractometer	Rigaku AFC5R
radiation	MoKα (0.71069 Å)
scan type	$\omega - 2\theta$
$2\theta_{max}$, deg	55.1
scan width, deg	1.84 + 0.35 tan θ
scan rate in ω, deg/min	10.0
no. of reflns measd	5610
no. of reflns obsd [$I > 3.00\sigma(I)$]	1181
no. of variables	272
R	0.065
R_w	0.070

rate was obtained from Nacalai Tesque. Acetonitrile (MeCN) used as a solvent was purified and dried by the standard procedure.[32] Acetonitrile-d_3 (CD_3CN) and chloroform-*d* were obtained from EURI SO-TOP, CEA, France.

Reaction Procedures and Analysis. The isolation of the cycloadduct of *t*-BuBNAH with *p*-benzoquinone was performed as follows. Typically, an MeCN solution of *t*-BuBNAH (2.0×10^{-2} M, 50 mL) was added to the reaction vessel that contained a solution (50 mL) of *p*-benzoquinone (Q; 2.0×10^{-2} M) in the presence of $Sc(OTf)_3$ (6.0×10^{-2} M) under an atmospheric pressure of argon. After the reaction was completed in 30 min, the resulting solution was evaporated. The residue was dissolved in diethyl ether and washed with deionized water. The organic layer was separated and the solvent was removed from the reaction mixture by distillation at 313 K under vacuum. The yellowish white solid residue was dried in a vacuum. The isolated yield of the cycloadduct (**1**, *t*-BuBNAH-Q) was 90%. The cycloadducts (**2**, BNAH-Q; **3**, *i*-PrBNAH-Q) were isolated in the same manner as **1**. The elemental analysis of isolated product (**1**) gave the satisfactory result. **1**: Anal. Calcd for $C_{23}H_{26}N_2O_3 \cdot 0.5(C_2H_5)_2O$: C, 72.26; H, 7.52; N, 6.74. Found: C, 72.05; H, 7.33; N, 6.86.

The isolated cycloadduct (**1**, *t*-BuBNAH-Q) were dissolved in MeCN and recrystallized from MeCN under an atmospheric pressure of diethyl ether vapor. The X-ray experiments were carried out on the Rigaku AFC-5R diffractometer with graphite-monochromatized Mo Kα radiation and a rotating anode generator. The absorption effect was corrected empirically on the basis of azimuthal scans of three reflections. The crystal structures were solved by direct method and refined by full-matrix least-squares techniques. The non-hydrogen atoms were refined anisotropically, while the hydrogen atoms located from the final stage of difference Fourier maps were included with isotropic thermal parameters. All the calculations were performed with the TEXSAN program package.[33] A summary of the fundamental crystal data and experimental parameters for structure determinations are given in Table 1. Atomic coordinates, thermal parameters, and intramolecular bond distances and angles have been deposited as Supporting Information.

(32) Perrin, D. D.; Armarego, W. L. F. *Purification of Laboratory Chemicals*; Butterworth-Heinemann: Oxford, UK, 1988.

(33) *TEXSAN, Single-Crystal Structure Analysis Software*, Version 5.0; Molecular Structure Corp.: The Woodlands, TX 77381, 1989.

For ^{1}H NMR measurements, a CD_3CN solution (0.4 mL) of *t*-BuBNAH (2.0×10^{-2} M) was added to an NMR tube that contained a CD_3CN solution (0.4 mL) of *p*-benzoquinone (2.0×10^{-2} M) in the presence of $Sc(OTf)_3$ (1.0×10^{-1} M) under an atmospheric pressure of argon. Then the solution was degassed by bubbling with argon for 5 min, and the NMR tube was sealed with a rubber septum. The products in the reaction of *t*-BuBNAH with *p*-benzoquinone derivatives in the presence of $Sc(OTf)_3$ are identified as a mixture of the corresponding cycloadduct (**4**, *t*-BuBNAH-(2,5-Cl_2Q); **5**, *t*-BuBNAH-(2,5-Me_2Q); **6**, *t*-BuBNAH-(2,6-Me_2Q)), BNA^+ (**7**). The products in the reaction of *t*-BuBNAH with Q in the presence of $Lu(OTf)_3$ (1.0×10^{-1} M), $Y(OTf)_3$ (1.0×10^{-1} M), or $Mg(ClO_4)_2$ (1.0 M) are identified as a mixture of the corresponding cycloadduct (**1**), BNA^+ (**7**), *t*-$BuBNA^+$ (**8**), and hydroquinone (**9**). The ^{1}H NMR measurements were performed with a Japan Electron Optics JNM-GSX-400 (400 MHz) NMR spectrometer at 300 K. Chemical shifts of ^{1}H NMR were expressed in parts per million downfield from tetramethylsilane as an internal standard ($\delta = 0$). FAB mass spectra were obtained with a JEOL JMS-DX303 HF mass spectrometer. **1**: UV−vis [MeCN, λ_{max}, nm (ϵ, M^{-1} cm^{-1})] 289 (1.5×10^4). FAB-MS: mass calcd. for $C_{23}H_{26}N_2O_3$, 379; found 379. ^{1}H NMR (CD_3CN) δ (ppm) 7.60 (s, 1H), 7.37−7.26 (m, 5H), 7.16 (s, 1H), 6.75 (d, $J = 2.4$ Hz, 1H), 6.62 (d, $J = 8.3$ Hz, 1H), 6.52 (ddd, $J = 8.3, 2.4, 1.0$ Hz, 1H), 5.7 (s, 2H), 5.48 (d, $J = 7.8$ Hz, 1H), 4.42 (d, $J = 14.7$ Hz, 1H), 4.17 (d, $J = 14.7$ Hz, 1H), 4.01 (d, $J = 7.8$ Hz, 1H), 2.96 (d, $J = 1.0$ Hz, 1H), 0.87 (s, 9H). **2**: FAB-MS: mass calcd. for $C_{19}H_{18}N_2O_3$, 322; found 322. ^{1}H NMR (CD_3CN) δ (ppm) 9.48 (s, 1H), 7.37−7.26 (m, 5H), 7.27 (s, 1H), 6.72 (d, $J = 2.6$ Hz, 1H), 6.58 (dd, $J = 8.4, 2.6$ Hz, 1H), 6.55 (d, $J = 8.4$ Hz, 1H), 5.91 (s, 2H), 5.41 (d, $J = 6.6$ Hz, 1H), 4.54 (d, $J = 15.4$ Hz, 1H), 4.40 (d, $J = 15.4$ Hz, 1H), 3.30 (d, $J = 7.3$ Hz, 1H), 2.58 (dd, $J = 15.8, 6.6$ Hz, 1H), 2.14 (dd, $J = 15.8, 7.3$ Hz, 1H). **3**: ^{1}H NMR (CD_3CN) δ (ppm) 7.95 (s, 1H), 7.39−7.33 (m, 5H), 6.66 (d, $J = 8.4$ Hz, 1H), 6.60 (d, $J = 2.6$ Hz, 1H), 6.57 (ddd, $J = 8.4, 2.6, 1.1$ Hz, 1H), 5.33 (d, $J = 7.0$ Hz, 1H), 4.62 (d, $J = 14.7$ Hz, 1H), 4.46 (d, $J = 14.7$ Hz, 1H), 3.94 (d, $J = 7.0$ Hz, 1H), 2.76 (d, $J = 1.1$ Hz, 1H), 1.82 (m, 1H), 1.00 (d, $J = 7.0$ Hz, 3H), 0.76 (d, $J = 7.0$ Hz, 3H). **4**: ^{1}H NMR (CD_3CN) δ (ppm) 8.07 (s, 1H), 7.42−7.32 (m, 5H), 6.83 (s, 1H), 5.53 (d, $J = 7.8$ Hz, 1H), 4.60 (d, $J = 14.3$ Hz, 1H), 4.48 (d, $J = 14.3$ Hz, 1H), 4.43 (d, $J = 7.8$ Hz, 1H), 3.56 (s, 1H), 0.87 (s, 9H). **5**: ^{1}H NMR (CD_3CN) δ (ppm) 8.09 (s, 1H), 7.41−7.31 (m, 5H), 6.43 (s, 1H), 5.39 (d, $J = 7.8$ Hz, 1H), 4.68 (d, $J = 14.3$ Hz, 1H), 4.46 (d, $J = 14.3$ Hz, 1H), 4.26 (d, $J = 7.8$ Hz, 1H), 2.98 (s, 1H), 2.17 (s, 3H), 2.05 (s, 3H), 0.89 (s, 9H). **6**: ^{1}H NMR (CD_3CN) δ (ppm) 8.11 (s, 1H), 7.44−7.34 (m, 5H), 6.46 (s, 1H), 5.42 (d, $J = 8.1$ Hz, 1H), 4.65 (d, $J = 14.3$ Hz, 1H), 4.48 (d, $J = 14.3$ Hz, 1H), 4.28 (d, $J = 8.1$ Hz, 1H), 2.94 (s, 1H), 2.25 (s, 3H), 2.12 (s, 3H), 0.90 (s, 9H). **7**: UV−vis [MeCN, λ_{max}, nm (ϵ, M^{-1} cm^{-1})] 266 (7.0×10^3). ^{1}H NMR (CD_3CN) δ (ppm) 9.17 (s, 1H), 8.86 (d, $J = 6.0$ Hz, 1H), 8.84 (d, $J = 7.9$ Hz, 1H), 8.14 (dd, $J = 7.9, 6.0$ Hz, 1H), 7.51−7.43 (m, 5H), 5.80 (s, 2H). **8**: ^{1}H NMR (CD_3CN) δ (ppm) 8.68 (s, 1H), 8.63 (d, $J = 6.8$ Hz, 1H), 8.08 (d, $J = 6.8$ Hz, 1H), 7.50−7.42 (m, 5H), 5.67 (s, 1H), 1.44 (s, 9H). **9**: UV−vis [MeCN, λ_{max}, nm (ϵ, M^{-1} cm^{-1})] 225 (6.6×10^3), 294 (3.5×10^3). ^{1}H NMR (CD_3CN) δ (ppm) 6.63 (s, 4H), 6.35 (s, 2H).

Spectral Measurements. The formation of rare-earth ion complexes with *t*-BuBNAH was examined from the change in the UV−vis spectra of *t*-BuBNAH (1.0×10^{-4} M) at $\lambda = 321$ nm in the presence of various concentrations of $Sc(OTf)_3$ (2.0×10^{-3} to 2.0×10^{-2} M), $Lu(OTf)_3$, $Y(OTf)_3$ (1.0×10^{-2} to 3.0×10^{-2} M), and $Mg(ClO_4)_2$ (1.0×10^{-4} to 5.0×10^{-1} M) using a Hewlett-Packard 8453 diode array spectrophotometer. The formation constants were obtained from the change in the UV−vis spectra due to the formation of the complexes: *t*-BuBNAH-Sc^{3+} ($\lambda_{max} = 364$ nm), *t*-BuBNAH-Lu^{3+} ($\lambda_{max} = 346$ nm), *t*-BuBNAH-Y^{3+} ($\lambda_{max} = 344$ nm), and *t*-BuBNAH-Mg^{2+} ($\lambda_{max} = 330$ nm).

Kinetic Measurements. Kinetic measurements of cycloaddition reactions of BNAH derivatives with substituted *p*-benzoquinones were performed on a Hewlett-Packard 8453 diode array spectrophotometer. Typically, a deaerated MeCN solution of *t*-BuBNAH (1.0×10^{-4} M) was added to a quartz cuvette (i.d. 10 mm) containing an MeCN solution of *p*-benzoquinone (2.0×10^{-3} M) and $Sc(OTf)_3$ (1.0×10^{-3} to 5.0 ×

10^{-2} M) by means of a microsyringe under argon with stirring. Rates of Sc^{3+}-catalyzed cycloaddition reactions of *t*-BuBNAH with substituted *p*-benzoquinones were monitored by measuring the decrease in absorption band at $\lambda_{max} = 364$ nm ($\epsilon_{max} = 1.1 \times 10^4$ M^{-1} cm^{-1}) due to the *t*-BuBNAH-Sc^{3+} complex in MeCN at 298 K in the dark. In the reaction of other BNAH derivatives with *p*-benzoquinone, the monitored absorption bands are located at $\lambda_{max} = 380$ nm ($\epsilon_{max} = 1.4 \times 10^4$ M^{-1} cm^{-1}) for BNAH and $\lambda_{max} = 372$ nm ($\epsilon_{max} = 1.3 \times 10^4$ M^{-1} cm^{-1}) for *i*-PrBNAH. Measurements of rates of electron-transfer reaction from CoTPP (8.0×10^{-6} to 1.2×10^{-5} M) to *p*-benzoquinone derivatives (2.6×10^{-4} M) in the presence and absence of $Sc(OTf)_3$ (5.0×10^{-3} to 7.6×10^{-2} M) were performed using a Union RA-103 stopped-flow spectrophotometer. The rates were monitored by the rise and decay of the absorption band at 434 and 412 nm due to $CoTPP^+$ and CoTPP in MeCN at 298 K, respectively. All kinetic measurements were carried out under pseudo-first-order conditions where concentrations of *p*-benzoquinones were maintained at more than 10-fold excess of CoTPP concentrations at 298 K. Pseudo-first-order rate constants were determined by least-squares linear curve fits using a personal computer. The pseudo-first-order plots were linear for 3 or more half-lives with the correlation coefficient $\rho > 0.999$.

Theoretical Calculations. Density functional calculations were performed on a COMPAQ DS20E computer using the spin-restricted B3LYP functional for the open shell $BNAH^{\bullet+}$.[34] The B3LYP geometry of $BNAH^{\bullet+}$ was determined by using the 6-31++G(d) basis and the Gaussian 98 program.[35] The $\langle S^2 \rangle$ value was determined as 0.773, indicating a good representation of the doublet state. Graphical output of the computational result was generated with the Cerius^2 software program developed by Molecular Simulations Inc.

Results and Discussion

Cycloaddition of NADH Analogues with *p*-Benzoquinone. Upon addition of *t*-BuBNAH (1.0×10^{-4} M) to a deaerated MeCN solution of *p*-benzoquinone (Q; 2.0×10^{-3} M) in the presence of $Sc(OTf)_3$ (1.0×10^{-2} M), the cycloaddition reaction of *t*-BuBNAH with Q occurs efficiently at 298 K (see the Experimental Section, R = Bu^t in eq 1). As the reaction

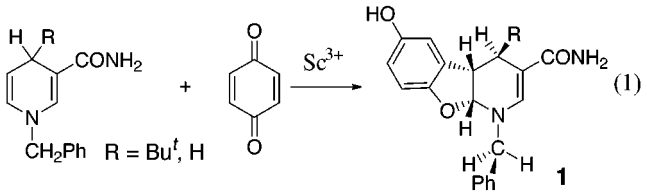

proceeds, the absorption bands due to *t*-BuBNAH ($\lambda_{max} = 364$ nm) and Q ($\lambda_{max} = 241$ nm) decrease, and these are accompanied by the appearance of a new absorption band ($\lambda_{max} = 320$ nm) due to the formation of cycloadduct **1** with three clear isosbestic points at 208, 262, and 337 nm (Figure 1). The same spectral changes were observed in the reaction of BNAH with Q (R = H in eq 1). The product absorption band at 320 nm seen in Figure 1 agrees with that for the previously reported water adduct of *N*-alkyl-1,4-dihydronicotinamide with a saturated C(5)−C(6) bond.[36] The cycloadducts **1** and **2** were isolated and a single crystal of **1** was obtained for X-ray crystal structure determination (see the Experimental Section). The ORTEP drawing of **1** is shown in Figure 2 (the crystallographic data are given in Table 1 and selected bond distances and angles for the crystal structures of **1** are given in the Supporting Information, S1).

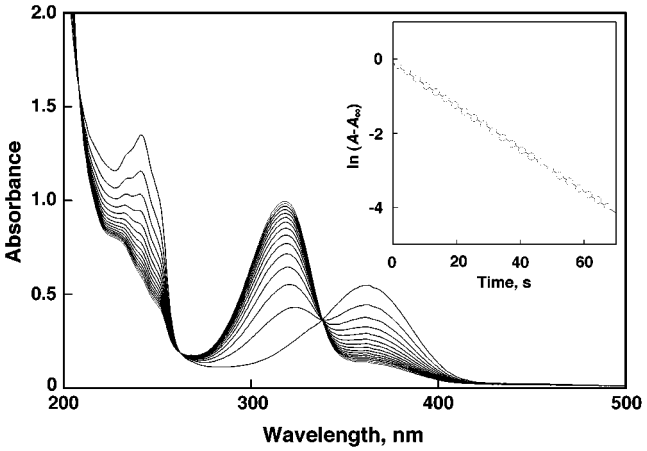

Figure 1. Spectral change observed in the cycloaddition reaction of *t*-BuBNAH (5.0×10^{-5} M) with *p*-benzoquinone (5.0×10^{-5} M) in the presence of $Sc(OTf)_3$ (5.0×10^{-2} M) in deaerated MeCN at 298 K (60 s interval). Inset: First-order plot based on the absorption change at $\lambda = 360$ nm in the cycloaddition reaction of *t*-BuBNAH (1.0×10^{-4} M) with Q (2.0×10^{-3} M) in the presence of $Sc(OTf)_3$ (2.0×10^{-2} M) in deaerated MeCN at 298 K (3 s interval).

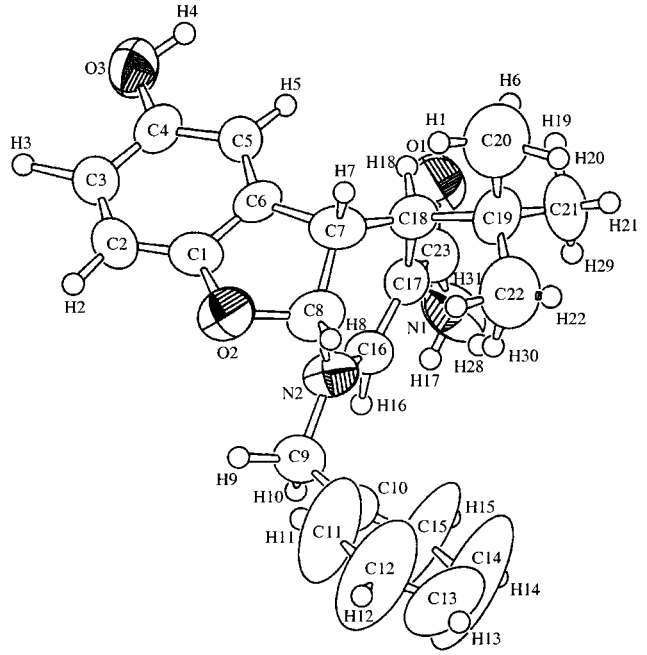

Figure 2. ORTEP drawing of the cycloadduct (**1**).

Complex Formation between NADH Analogues and $Sc(OTf)_3$. The UV−vis absorption spectra of *t*-BuBNAH in MeCN are significantly affected by the addition of metal ions as shown in Figure 3. The absorption band at 321 nm due to *t*-BuBNAH (1.0×10^{-4} M) is red shifted and the new absorption band at 364 nm appeared with a distinct isosbestic point at 327 nm in the presence of $Sc(OTf)_3$. Such spectroscopic changes

(34) Becke, A. D. *J. Chem. Phys.* **1993**, *98*, 5648−5652.

(35) Frisch, M. J.; Trucks, G. W.; Schlegel, H. B.; Scuseria, G. E.; Robb, M. A.; Cheeseman, J. R.; Zakrzewski, V. G.; Montgomery, J. A., Jr.; Stratmann, R. E.; Burant, J. C.; Dapprich, S.; Millam, J. M.; Daniels, A. D.; Kudin, K. N.; Strain, M. C.; Farkas, O.; Tomasi, J.; Barone, V.; Cossi, M.; Cammi, R.; Mennucci, B.; Pomelli, C.; Adamo, C.; Clifford, S.; Ochterski, J.; Petersson, G. A.; Ayala, P. Y.; Cui, Q.; Morokuma, K.; Malick, D. K.; Rabuck, A. D.; Raghavachari, K.; Foresman, J. B.; Cioslowski, J.; Ortiz, J. V.; Baboul, A. G.; Stefanov, B. B.; Liu, G.; Liashenko, A.; Piskorz, P.; Komaromi, I.; Gomperts, R.; Martin, R. L.; Fox, D. J.; Keith, T.; Al-Laham, M. A.; Peng, C. Y.; Nanayakkara, A.; Gonzalez, C.; Challacombe, M.; Gill, P. M. W.; Johnson, B.; Chen, W.; Wong, M. W.; Andres, J. L.; Gonzalez, C.; Head-Gordon, M.; Replogle, E. S.; Pople, J. A. *Gaussian 98*, Revision A.7; Gaussian, Inc.; Pittsburgh, PA, 1998.

(36) (a) Johnston, C. C.; Gardner, J. L.; Suelter, C. H.; Metzler, D. E. *Biochemistry* **1963**, *2*, 689. (b) Yoon, C.-J.; Ikeda, H.; Kojin, R.; Ikeda, T.; Toda, F. *J. Chem. Soc., Chem. Commun.* **1986**, 1080.

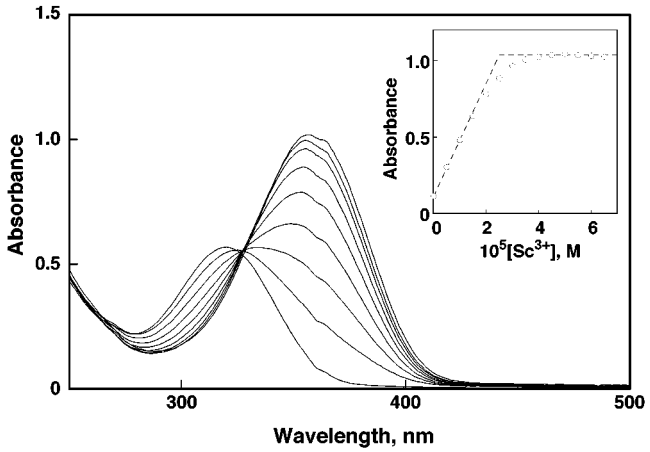

Figure 3. Spectral change observed upon addition of $Sc(OTf)_3$ (0−4.0×10^{-5} M) to a deaerated MeCN solution containing *t*-BuBNAH (1.0×10^{-4} M). Inset: The absorption change at $\lambda = 360$ nm.

shown in Figure 3 are ascribed to formation of the complex between *t*-BuBNAH and $Sc(OTf)_3$. The stoichiometry is established by spectral titration (see the inset of Figure 3), where *t*-BuBNAH forms a 4:1 complex with Sc^{3+} (eq 2).[37] The same spectral changes were observed for the complex formation of

$$4\ t\text{-BUBNAH} + Sc^{3+} \rightleftarrows (t\text{-BuBNAH})_4Sc^{3+} \qquad (2)$$

BNAH ($\lambda_{max} = 348$ nm) with Sc^{3+} ($(BNAH)_4Sc^{3+}$; $\lambda_{max} = 380$ nm). Other rare earth metal ions (Lu^{3+}, Y^{3+}) also form complexes with *t*-BuBNAH ($(t\text{-BuBNAH})_4Lu^{3+}$, $\lambda_{max} = 346$ nm; $(t\text{-BuBNAH})_4Y^{3+}$, $\lambda_{max} = 344$ nm).

Kinetics of Sc^{3+}-Catalyzed Cycloaddition and Electron-Transfer Reactions. The rates of reactions of *t*-BuBNAH with Q in the presence of Sc^{3+} (2.0×10^{-2} M) in MeCN at 298 K were determined by monitoring the disappearance of absorbance due to the *t*-BuBNAH-Sc^{3+} complex ($\lambda_{max} = 364$ nm, $\epsilon_{max} = 1.1 \times 10^4$ M^{-1} cm^{-1}). The rates obeyed pseudo-first-order kinetics in the presence of a large excess of Q and Sc^{3+} relative to the concentration of *t*-BuBNAH (see inset of Figure 1). The pseudo-first-order rate constant increases proportionally with Q concentration (see the Supporting Information, S3). Thus, the rate exhibits the second-order kinetics showing a first-order dependence on each reactant concentration.

The dependence of the observed second-order rate constant (k_{obs}) on [Sc^{3+}] was examined for the cycloaddition reactions of *t*-BuBNAH with Q at various concentrations of Sc^{3+}. The k_{obs} value increases with an increase in [Sc^{3+}] to exhibit a first-order dependence on [Sc^{3+}] at low concentrations, changing to a second-order dependence at high concentrations as shown in Figure 4a.

Such a mixture of first-order and second-order dependence on [Sc^{3+}] is also observed in electron transfer from CoTPP (TPP = tetraphenylporphyrin dianion) to Q. No electron transfer from CoTPP to Q has occurred in MeCN at 298 K. In the presence of $Sc(OTf)_3$, however, an efficient electron transfer from CoTPP to Q occurs to yield $CoTPP^+$ (eq 3). The electron-transfer rates

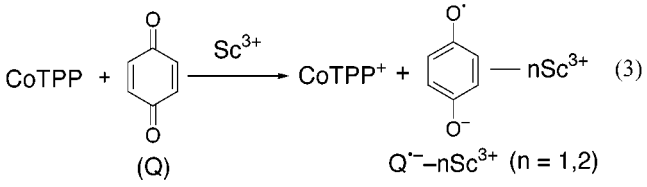

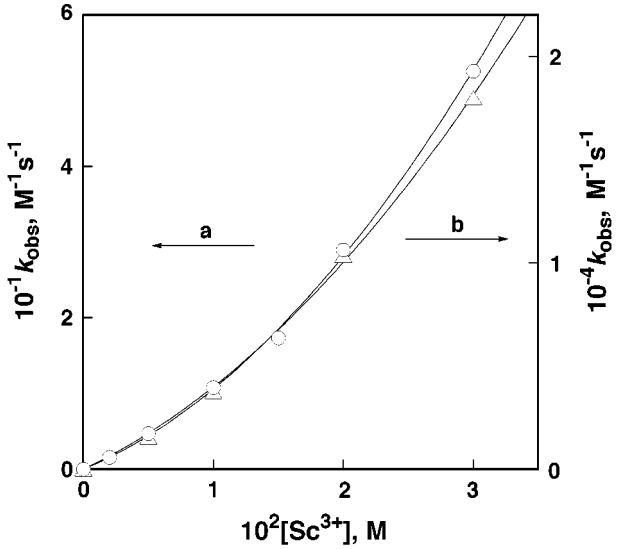

Figure 4. Dependence of k_{obs} on [Sc^{3+}] for (a) the cycloaddition reaction of *t*-BuBNAH (1.0×10^{-4} M) with *p*-benzoquinone (2.0×10^{-3} M) and (b) electron transfer from CoTPP (8.0×10^{-6} M) to *p*-benzoquinone (2.6×10^{-4} M) in the presence of $Sc(OTf)_3$ in deaerated MeCN at 298 K.

obeyed second-order kinetics, showing a first-order dependence on each reactant concentration. The dependence of the observed electron-transfer rate constant (k_{et}) on [Sc^{3+}] was also examined for electron transfer from CoTPP to Q at various concentrations of Sc^{3+}. The results are shown in Figure 4b, where the k_{et} value increases linearly with [Sc^{3+}] to show a first-order dependence on [Sc^{3+}] at low concentrations, changing to a second-order dependence at high concentrations as is the case of the Sc^{3+}-catalyzed cycloaddition of *t*-BuBNAH with Q in Figure 4a.

There is no interaction between Q and Sc^{3+} as indicated by the lack of spectral change of Q in the presence of Sc^{3+}. In such a case, the acceleration of electron transfer from CoTPP to Q is ascribed to the complexation of Sc^{3+} with $Q^{\bullet-}$. Since there are two carbonyl oxygens which can interact with Sc^{3+}, $Q^{\bullet-}$ may form not only a 1:1 complex ($n = 1$ in eq 3) but also a 1:2 complex ($n = 2$ in eq 3) with Sc^{3+}. The complex formation of $Q^{\bullet-}$ and Sc^{3+} should result in the positive shift of the one-electron reduction potential of Q (E_{red}) and the Nernst equation is given by eq 4, where E^0_{red} is the one-electron reduction potential of Q in the absence of Sc^{3+}, where K_1

$$E_{red} = E^0_{red} + (2.3RT/F)\log K_1[Sc^{3+}](1 + K_2[Sc^{3+}]) \qquad (4)$$

and K_2 are the formation constants for the 1:1 and 1:2 complexes between $Q^{\bullet-}$ and Sc^{3+}, respectively. Since Sc^{3+} has no effect on the oxidation potential of CoTPP, the free energy change of electron transfer from CoTPP to Q in the presence of Sc^{3+} (ΔG_{et}) can be expressed by eq 5, where ΔG^0_{et} is the free energy change in the absence of Sc^{3+}. Thus, electron transfer from

$$\Delta G_{et} = \Delta G^0_{et} - (2.3RT)\log(K_1[Sc^{3+}] + K_1K_2[Sc^{3+}]^2) \qquad (5)$$

CoTPP to Q becomes more favorable energetically with an increase in concentration of Sc^{3+}. If such a change in the energetics is directly reflected in the transition state of electron transfer, the dependence of the observed rate constant of electron

(37) The rate of formation of the complex may be diffusion-limited because the rate was too fast to be followd with a stopped-flow technique.

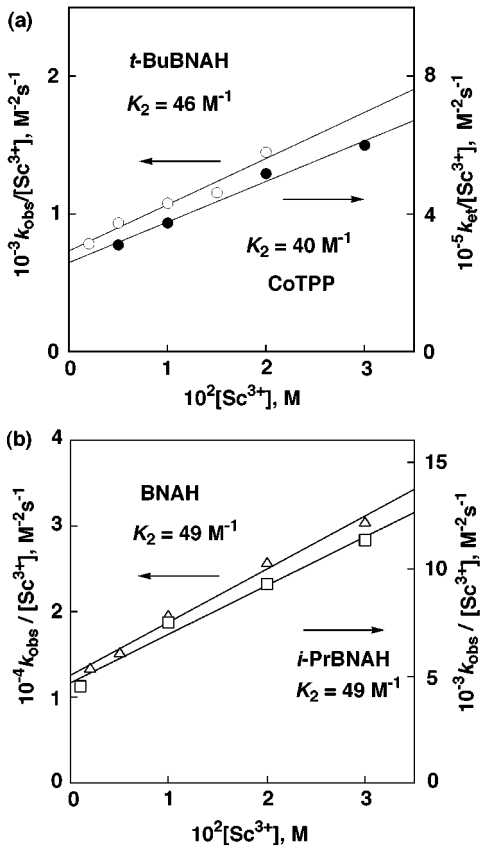

Figure 5. (a) Plots of $k_{obs}/[Sc^{3+}]$ vs $[Sc^{3+}]$ for the cycloaddition reaction (○) of *t*-BuBNAH (1.0×10^{-4} M) with Q (2.0×10^{-3} M) and electron transfer from CoTPP to Q (●) in the presence of $Sc(OTf)_3$ in deaerated MeCN at 298 K. (b) Plots of $k_{obs}/[Sc^{3+}]$ vs $[Sc^{3+}]$ for the cycloaddition reaction of BNAH *i*-PrBNAH (1.0×10^{-4} M) with Q (2.0×10^{-3} M) in the presence of $Sc(OTf)_3$ in deaerated MeCN at 298 K.

transfer (k_{et}) on $[Sc^{3+}]$ is derived from eq 5, as given by eq 6, where k_0 is the rate constant in the absence of Sc^{3+}. The validity of eq 6 is confirmed by the linear plot of $k_{et}/[Sc^{3+}]$ vs $[Sc^{3+}]$ for the Sc^{3+}-promoted electron transfer from CoTPP to Q as

$$k_{et}/[Sc^{3+}] = k_0K_1(1 + K_2[Sc^{3+}]) \quad (6)$$

shown in Figure 5a (closed circles).[38] From the slopes and intercepts are obtained the K_2 value, which is listed in Table 2, together with the k_0K_1 value.

There is a striking similarity with respect to the dependence of k_{et} (or k_{obs}) on $[Sc^{3+}]$ between the electron-transfer reactions from CoTPP to Q (Figure 4a) and the cycloaddition reaction of *t*-BuBNAH with Q (Figures 4b), despite the large difference in their reactivities. Thus, the same plot as in eq 6 for the Sc^{3+}-promoted electron transfer from CoTPP to Q can be applied for the Sc^{3+}-catalyzed cycloaddition reactions of *t*-BuBNAH with Q as shown in Figure 5a (open circles). The K_2 value for the 1:2 complex formation between $Q^{\bullet-}$ and Sc^{3+} is obtained from the linear plot as listed in Table 2. The dependence of k_{obs} on $[Sc^{3+}]$ was also determined for the cycloaddition reactions of BNAH and *i*-PrBNAH with Q. The K_2 values are also determined from the linear plots of $k_{obs}/[Sc^{3+}]$ vs $[Sc^{3+}]$ in Figure 5b and they are listed in Table 2. These K_2 values (46−49 M^{-1}) are essentially the same within experimental error irrespective of different reactivities of NADH analogues (see k_0K_1 values in Table 2). In each case, the K_2 value agrees within the experimental error with the value (40 M^{-1}) determined from the Sc^{3+}-promoted electron transfer reaction (Table 2). Such an agreement strongly indicates that the catalytic function of Sc^{3+} in the cycloaddition reactions of NADH analogues with Q is essentially the same as the function in electron transfer from CoTPP to Q. This means that the cycloaddition of the NADH analogues with Q proceeds via a rate-determining electron transfer from NADH analogues to Q, which is accelerated by formation of the 1:1 and 1:2 complex between $Q^{\bullet-}$ with Sc^{3+} as in the case of an electron transfer from CoTPP to Q.

The K_2 value may change depending on the substituents on Q. This was examined by determining the dependence of k_{obs} and k_{et} on $[Sc^{3+}]$ for the cycloaddition of *t*-BNAH with substituted *p*-benzoquinone derivatives and also the electron transfer from CoTPP to the same *p*-benzoquinone derivatives. The linear plots of $k_{obs}/[Sc^{3+}]$ vs $[Sc^{3+}]$ and $k_{et}/[Sc^{3+}]$ vs $[Sc^{3+}]$ are shown in Figure 6, parts a and b, respectively. The K_2 values determined from the linear plots are also listed in Table 2. The K_2 value (25 M^{-1}) determined in the Sc^{3+}-promoted electron transfer from CoTPP to a *p*-benzoquinone derivative with electron-withdrawing substituents (2,5-dichloro-*p*-benzoquinone) is smaller than the corresponding K_2 value of *p*-benzoquinone (40 M^{-1}) as expected from the weaker basicity of the radical anion with the electron-withdrawing substituents as compared to the basicity of the unsubstituted semiquinone radical anion. In each case, the K_2 value determined from the Sc^{3+}-catalyzed cycloaddition reactions with the *p*-benzoquinone derivative agrees with the value determined from the corresponding Sc^{3+}-promoted electron-transfer reaction (Table 2). Such an agreement confirms that the Sc^{3+}-catalyzed cycloaddition of the NADH analogues with the *p*-benzoquinone derivative (X-Q) proceeds via the rate-determining Sc^{3+}-promoted electron transfer from NADH analogues to X-Q.

Detection of Semiquinone Radical Anion-Sc^{3+} Complexes. The 1:2 complex formation between $Q^{\bullet-}$ and Sc^{3+} has been confirmed by observation of the ESR spectrum of the $Q^{\bullet-}$-$2Sc^{3+}$ complex which shows the superhyperfine structure due to the interaction of $Q^{\bullet-}$ with two equivalent Sc nuclei. Since the $Q^{\bullet-}$-$2Sc^{3+}$ complex is unstable because of the facile disproportionation reaction, the complex was generated in photoinduced electron transfer from dimeric 1-benzyl-1,4-dihydronicotinamide $[(BNA)_2]$[39,40] to Q at low temperatures. The $(BNA)_2$ is known to act as a unique electron donor to produce the radical anions of electron acceptors.[40] The photochemical reaction was carried out in an ESR cavity where an ESR tube containing a propionitrile (EtCN) solution of $(BNA)_2$, Q, and Sc^{3+} was irradiated with a mercury lamp at 203 K. Propionitrile was used instead of MeCN to avoid freezing the solvent at 203 K. The observed ESR spectrum of $Q^{\bullet-}$ in the presence of Sc^{3+} (4.4×10^{-2} M) is shown in Figure 7a. The well-resolved 19 lines of the spectrum clearly indicate the hyperfine splitting (a(H)) due to 4 protons of semiquinone radical anions and superhyperfine splitting (a(Sc)) of two equivalent Sc^{3+} nuclei ($I = {}^7/_2$). The coupling constants are almost the same between a(H) and a(Sc), resulting in the overall nuclear spin = 9 that causes 19 lines. The computer simulation spectrum with a(H) = 1.15 G, a(Sc) = 1.15 G with a line width (ΔH_{msl}) = 0.50 G is shown in Figure 5b for comparison. The observed ESR spectrum in Figure 5b clearly demonstrates the formation of the 1:2 complex between

(38) Since Sc^{3+} is bound to the reaction product (eq 3), the reaction is called "Sc^{3+}-promoted" electron transfer. In the case of the cycloaddition reactions (eq 1), Sc^{3+} acts as a real catalyst.

(39) Patz, M.; Kuwahara, Y.; Suenobu, T.; Fukuzumi, S. *Chem. Lett.* **1997**, 567.

(40) Fukuzumi, S.; Suenobu, T.; Patz, M.; Hirasaka, T.; Itoh, S.; Fujitsuka, M.; Ito, O. *J. Am. Chem. Soc*. **1998**, *120*, 8060.

Table 2. Rate Constants (k_0K_1) of Sc^{3+}-Catalyzed Cycloaddition Reactions of NADH Analogues with *p*-Benzoquinone Derivatives (X-Q) and the Formation Constants (K_2) of the X-$Q^{\bullet-}$-2Sc^{3+} Complexes in Deaerated MeCN at 298 K[a]

NADH analogue	*p*-benzoquinone derivative	k_0K_1,[b] $M^{-2}\,s^{-1}$	K_2,[b] M^{-1}
t-BuBNAH	*p*-benzoquinone	7.3×10^2 (2.7×10^5)	4.6×10 (4.0×10)
i-PrBNAH	*p*-benzoquinone	4.7×10^3 (2.7×10^5)	4.9×10 (4.0×10)
BNAH	*p*-benzoquinone	1.3×10^4 (2.7×10^5)	4.9×10 (4.0×10)
BNAH	2,5-dichloro-*p*-benzoquinone	2.2×10^2 (9.3×10^5)	2.6×10 (2.5×10)
BNAH	2,5-dimethyl-*p*-benzoquinone	6.6×10 (1.1×10^5)	4.8×10 (4.3×10)
BNAH	2,6-dimethyl-*p*-benzoquinone	1.0×10 (8.0×10^4)	4.3×10 (4.7×10)

[a] K_1 and K_2 are the formation constants for the 1:1 and 1:2 complexes between $Q^{\bullet-}$ and Sc^{3+}, respectively; k_0 is the rate constant in the absence of Sc^{3+} (see text). [b] Determined from the dependence of k_{obs} on [Sc^{3+}] based on eq 6. The experimental error is 10%. Values in parentheses are those determined for Sc^{3+}-promoted electron transfer from CoTPP to X-Q.

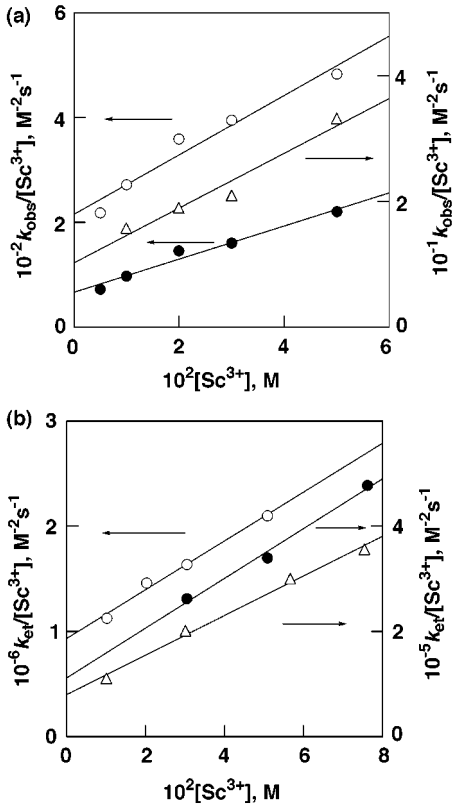

Figure 6. Plots of $k_{obs}/[Sc^{3+}]$ vs [Sc^{3+}] for (a) the cycloaddition reactions of *t*-BuBNAH and (b) electron-transfer reactions of CoTPP with 2,5-dichloro-*p*-benzoquinone, 2,5-dimethyl-*p*-benzoquinone, and 2,6-dimethyl-*p*-benzoquinone in MeCN at 298 K.

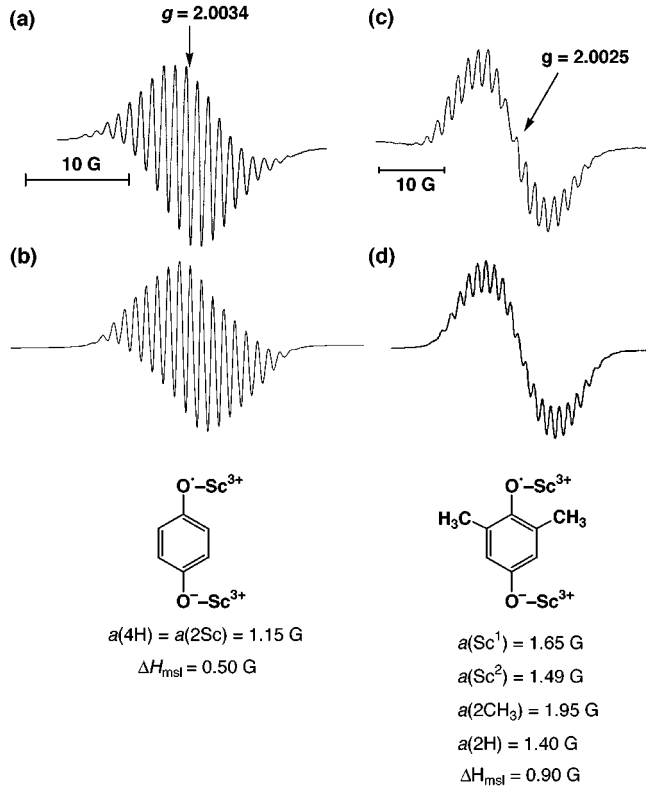

Figure 7. (a) ESR spectrum of a propionitrile solution containing $(BNA)_2$ (1.6×10^{-2} M), *p*-benzoquinone (4.9×10^{-2} M), and $Sc(OTf)_3$ (4.4×10^{-2} M) irradiated with a high-pressure mercury lamp at 203 K. (b) Computer simulation spectrum with $g = 2.0034$, a(4H) = a(2Sc) = 1.15 G, and $\Delta H_{msl} = 0.50$ G.

$Q^{\bullet-}$ and Sc^{3+} (eq 7).[41] Similarly, the 1:2 complex formation

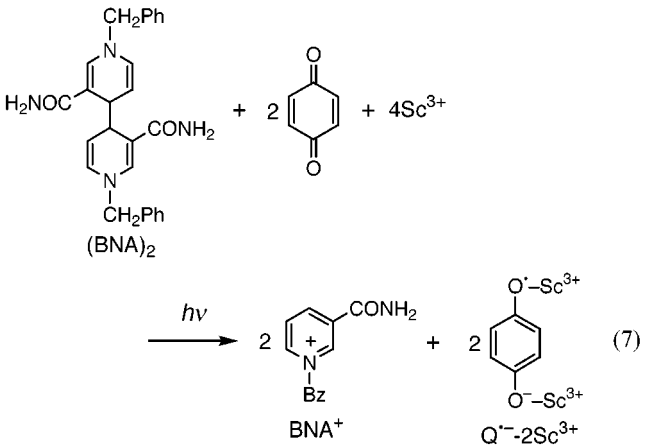

between the radical anion of 2,6-dimethyl-*p*-benzoquinone (2,5-$Me_2Q^{\bullet-}$) and Sc^{3+} is confirmed by the ESR spectra of the 2,5-$Me_2Q^{\bullet-}$-2Sc^{3+} complex and the corresponding computer simulation spectra as shown in Figure 7, parts c and d, respectively.

Mechanisms of Metal Ion-Catalyzed Cycloaddition vs Hydride Transfer Reactions. In the cycloaddition reactions of *t*-BNAH and BNAH with Q (eqs 1 and 2, respectively), the C−H bond of Q is cleaved to yield the adducts. If the Sc^{3+}-promoted electron transfer from *t*-BNAH and BNAH to Q is the rate-determining step as indicated from the catalytic function of Sc^{3+} in comparison with that in the electron-transfer reaction with CoTPP (vide supra), the C−H bond cleavage process should be fast enough that no primary kinetic isotope effect can be observed. This is confirmed by the primary kinetic deuterium isotope effect (k_H/k_D) in the Sc^{3+}-catalyzed cycloaddition reaction of *t*-BuBNAH with Q, where the deuterium-

(41) The 1:2 complex between $Q^{\bullet-}$ and Sc^{3+} is exclusively formed at 203 K probably because of the large K_2 value at the low temperature as compared to the value at 298 K in Table 2.

Table 3. Yields of Products in Reactions of BNAH and *t*-BuBNAH with *p*-Benzoquinone in the Presence of a Metal Ion [$Sc(OTf)_3$, $Lu(OTf)_3$, $Y(OTf)_3$ (1.0×10^{-1} M), or $Mg(ClO_4)_2$ (1.0 M)] and Rate Constants (k_{obs}) of Reactions of *t*-BuBNAH (1.0×10^{-4} M) with *p*-Benzoquinone (2.0×10^{-3} M) in the Presence of Metal Ions (3.0×10^{-2} M) in Deaerated MeCN at 298 K

metal ion	yield (%)					$10^2 k_{obs}$, $M^{-1} s^{-1}$
	t-BuBNAH			BNAH		
	cycloadduct	BNA^+	*t*-$BuBNA^+$	cycloadduct	BNA^+	
Sc^{3+}	100	0	0	100	0	5.3×10^3
Lu^{3+}	72	28	0	33	67	6.1
Y^{3+}	59	41	0	21	79	3.1
Mg^{2+}	35	5	60	7	93	0.26[a]

[a] $Mg(ClO_4)_2$ (5.0×10^{-1} M).

labeled Q (Q-2,3,5,6-d_4) was utilized (eq 8). The k_H/k_D value is

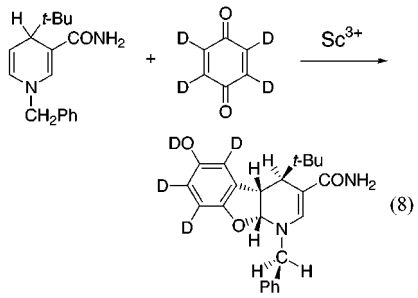

(8)

unity at various Sc^{3+} concentrations (see the Supporting Information, S3). The k_H/k_D value for the Sc^{3+}-catalyzed cycloaddition reaction of BNAH with Q (Q-2,3,5,6-d_4) is also found to be unity at various Sc^{3+} concentrations (S3).

When Sc^{3+} is replaced by other metal ions such as Lu^{3+} [$Lu(OTf)_3$], Y^{3+} [$Y(OTf)_3$], or Mg^{2+} [$Mg(ClO_4)_2$] in the reaction of *t*-BuBNAH with Q, BNA^+ is formed together with the cycloadduct. The product yields are listed in Table 3. In the case of Mg^{2+}, the cycloaddition is no longer the main reaction, but a hydride transfer from *t*-BuBNAH to Q occurs to yield *t*-BNA^+ as the major product (60%) (Table 3). Thus, there are three types of reactions depending on the type of metal ion, as shown in Scheme 1, where one is the cycloaddition reaction, another is a transfer of *t*-Bu^- to Q, and the other is a hydride transfer from *t*-BuBNAH to Q. The catalytic reactivity is also changed drastically by the type of metal ions employed as the catalyst. The k_{obs} values were determined from the rates of disappearance of the absorption band due to *t*-BuBNAH-metal ion complexes in the reactions with Q in MeCN at 298 K. The dependence of k_{obs} on the metal ion concentration is shown in Figure 8. The k_{obs} values thus determined in the presence of a fixed metal ion concentration are listed in Table 3, where the k_{obs} decreases in order $Sc^{3+} \gg Lu^{3+} > Y^{3+} > Mg^{2+}$. This order agrees with the Lewis acidity of the metal ions.[42]

When *t*-BuBNAH is replaced by BNAH in the reaction with Q catalyzed by metal ions other than Sc^{3+}, a hydride transfer from BNAH to Q becomes the main reaction and the yield of BNA^+ increases in order Lu^{3+} (67%) < Y^{3+} (79%) < Mg^{2+} (93%) with a decrease in the Lewis acidity of the metal ion (Table 3). The reaction mechanisms of Mg^{2+}-catalyzed hydride transfer from BNAH to Q have been extensively studied chemically or electrochemically.[3,12] However, this is the first report disclosing the minor reaction pathway of the cycloaddition (7%) competing with the major hydride transfer reaction pathway (93%).

(42) Fukuzumi, S.; Ohkubo, K. *Chem. Eur. J.* **2000**, *6*, 4532.

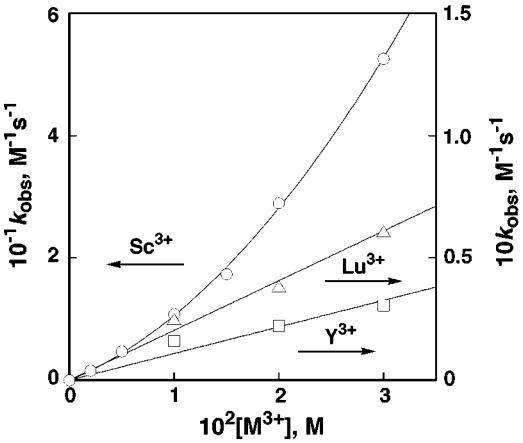

Figure 8. Dependence of k_{obs} on $[M^{3+}]$ for the reaction of *t*-BuBNAH (1.0×10^{-4} M) with Q (2.0×10^{-3} M) in the presence of $Sc(OTf)_3$ (○), $Lu(OTf)_3$ (△), or $Y(OTf)_3$ (●) in deaerated MeCN at 298 K.

Scheme 1

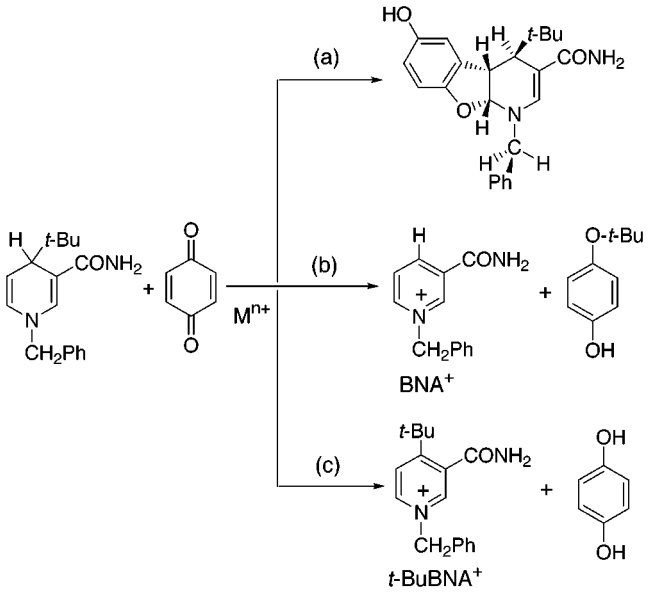

The Mg^{2+}-catalyzed hydride transfer from BNAH to Q is known to proceed via a Mg^{2+}-promoted electron transfer from BNAH to Q, followed by a proton transfer from the resulting $BNAH^{\bullet+}$ to the $Q^{\bullet-}$-$2Mg^{2+}$ complex and the subsequent fast electron transfer from $BNA^{\bullet}$ to QH^--Mg^{2+}.[3a,12] The change in the type of reaction depending on the Lewis acidity of the metal ion in Scheme 1 is well accommodated in the electron-transfer mechanism in Scheme 2. The initial rate-determining electron transfer from *t*-BuBNAH to Q results in the formation of a radical ion pair (*t*-$BuBNAH^{\bullet+}$ and $Q^{\bullet-}$) where $Q^{\bullet-}$ forms 1:1 and 1:2 complexes with Sc^{3+}.[43] This is followed by fast radical coupling between $Q^{\bullet-}$ and *t*-$BuBNAH^{\bullet+}$ to give the zwitterionic intermediate that is eventually converted to the cycloadduct **1**. In the same manner, the Sc^{3+}-catalyzed cycloaddition reaction of BNAH with Q proceeds via the Sc^{3+}-promoted electron transfer from BNAH to Q. The spin density distribution of $BNAH^{\bullet+}$ calculated by using a density functional theory at the UB3LYP/6-31++G* level is shown in Figure 9. There is a large spin density ($\rho = 0.466$) at C(5) of $BNAH^{\bullet+}$. Thus, the radical coupling of C(5) of $BNAH^{\bullet+}$ with $Q^{\bullet-}$-$2M^{n+}$ may occur

(43) The NADH analogue (*t*-BuBNAH) in Scheme 2 forms a 4:1 complex with Sc^{3+} (eq 2), which reacts with Q, since the absorption maximum (364 nm) due to the complex remains the same during the reaction. For clarity the complex formation is omitted in Scheme 2.

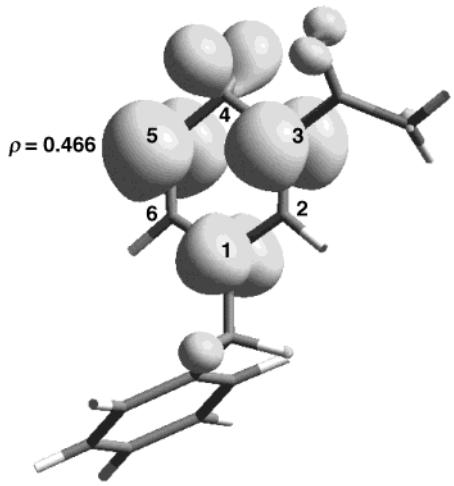

Figure 9. Spin density distribution of $BNAH^{\bullet+}$ calculated by using a density functional theory at the UB3LYP/6-31++G* level.

Scheme 2

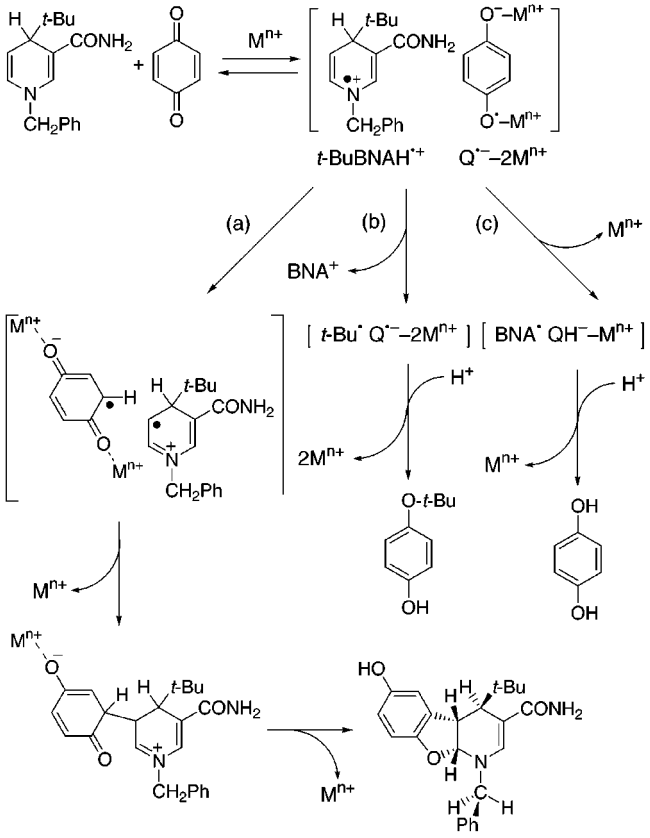

efficiently (pathway a) in competition with the proton transfer from $BNAH^{\bullet+}$ to $Q^{\bullet-}$-$2M^{n+}$, which leads to the overall hydride transfer from BNAH to Q (pathway c). With decreasing the Lewis acidity of the metal ion, the metal ion-promoted electron transfer from BNAH to Q is decelerated because of the weaker binding of the metal ion with $Q^{\bullet-}$ as shown in Table 3. On the other hand, the proton transfer from $BNAH^{\bullet+}$ to the $Q^{\bullet-}$-$2M^{n+}$ complex is accelerated with decreasing the Lewis acidity to the metal ion (M^{n+}) due to the stronger basicity of the $Q^{\bullet-}$-$2M^{n+}$ complex. This may be the reason the hydride transfer pathway from BNAH to Q becomes dominant in the presence of a much weaker Lewis acid (e.g., Mg^{2+}) as compared to the selective cycloaddition reaction in the presence of Sc^{3+} (see the product yields in Table 3).[44]

In the case of *t*-BuBNAH, the C(4)−C bond of *t*-$BuBNAH^{\bullet+}$ is known to be cleaved to produce *t*-$Bu^{\bullet}$,[9g,27,40] which can combine with $Q^{\bullet-}$-$2M^{n+}$ (pathway b in Scheme 2), leading to the overall transfer of *t*-Bu^{-} to Q. With decreasing the Lewis acidity of the metal ion, the C(4)−C bond cleavage of *t*-$BNAH^{\bullet+}$ may also be accelerated due to the stronger basicity of the $Q^{\bullet-}$-$2M^{n+}$ complex. This may be the reason the overall transfer of *t*-Bu^{-} to Q (pathway b in Scheme 2) starts to compete with the cycloaddition pathway as the Lewis acidity of the metal ion is decreased (see the product yields in Table 3). The deprotonation of *t*-$BuBNAH^{\bullet+}$ may be much slower as compared to that of $BNAH^{\bullet+}$, since the replacement of one active hydrogen of NADH analogues by an alkyl group is known to retard the deprotonation of the radical cations.[4d,e,9g] Thus, only in the case of Mg^{2+}, which is the weakest Lewis acid employed as a catalyst in this study, does the proton transfer from *t*-BuBNAH to $Q^{\bullet-}$-$2M^{n+}$ (pathway c in Scheme 2) compete with the radical coupling process (pathway a in Scheme 2) to yield the hydride transfer product (60% yield in Table 3).

Summary and Conclusions

Novel cycloaddition reactions have been accomplished via the Sc^{3+} ion-catalyzed reaction of BNAH or substituted BNAH with *p*-benzoquinones in MeCN at room temperature. The crystal structure of the cycloadduct between BNAH derivatives (*t*-BuBNAH) and *p*-benzoquinone was determined for the first time.

The dependence of the rate constants of cycloaddition reactions of BNAH analogues with *p*-benzoquinones on Sc^{3+} concentration agrees well with those of the electron-transfer rate constants from CoTPP to the corresponding *p*-benzoquinones on Sc^{3+} concentration. This indicates that the addition proceeds via the Sc^{3+}-promoted electron transfer from BNAH analogues to Q, which is the rate-determining step. It has been shown for the first time how the hydride transfer pathway is changed to the cycloaddition pathway through the metal ion-promoted electron transfer from NADH analogues to *p*-benzoquinone derivatives depending on the Lewis acidity of the metal ion (Scheme 2).

Acknowledgment. This work was partially supported by a Grant-in-Aid for Scientific Research Priority Area (Nos. 11228205 and 13031059) from the Ministry of Education, Culture, Sports, Science and Technology, Japan.

Supporting Information Available: Selected bond distances and angles for the crystal structures of **1** (S1), a plot of the pseudo-first-order rate constant vs [Q] (S2), and plots of k_H/k_D vs [Sc^{3+}] (S3) (PDF); an X-ray crystallographic file (CIF). This material is available free of charge via the Internet at http://pubs.acs.org.

JA016370K

(44) The cation charge/radius ratio or d-orbitals of Sc^{3+} may also help to stabilize the cycloaddition activated complex.